# Electronic Supplementary Information

# Large-Area All-Perovskite-Based Coplanar Photoelectrodes for Scaled-Up Solar Hydrogen Production

Wooyong Jeong, Gyumin Jang, Juwon Yun, Chang Seop Jeong, Young Sun Park, Hyungsoo Lee, Jaehyun Son, Chan Uk Lee, Jeongyoub Lee, Junwoo Lee, Seongyeon Yang, Soobin Lee, Subin Moon and Jooho Moon*

Department of Materials Science and Engineering, Yonsei University, Seoul 03722, Republic of Korea

*E-mail: jmoon@yonsei.ac.kr

**Keywords**: large-scale perovskite, antisolvent bathing, perovskite photoelectrode, photoelectrochemical water splitting

## Supplementary Figures

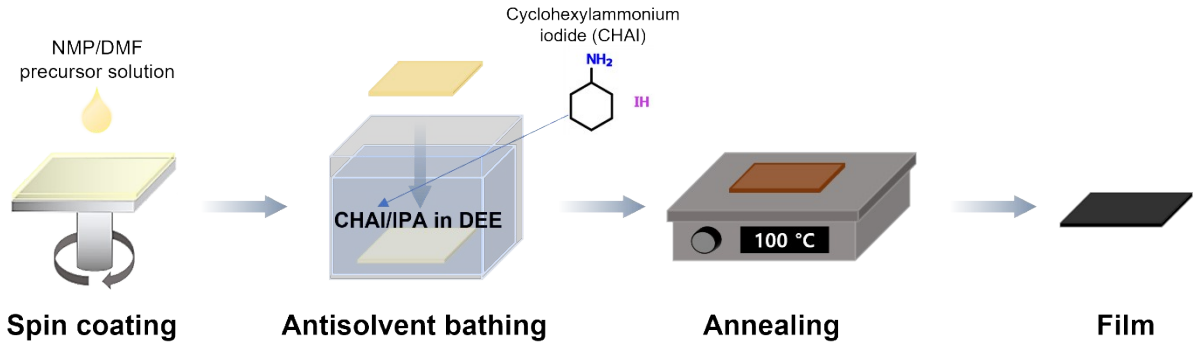


**Fig. S1** Schematic of perovskite film fabrication using a bathing method involving an additive-added antisolvent.

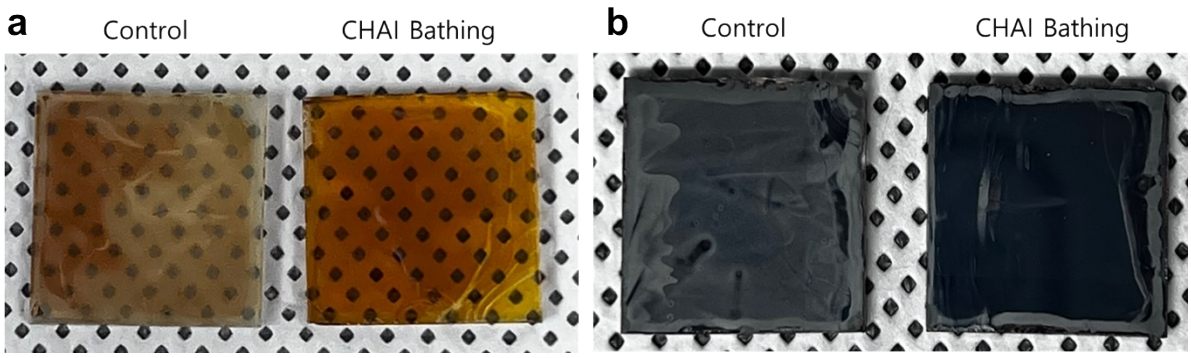


**Fig. S2** Digital photographs of the control and CHAI-bathed perovskite films (a) before and (b) after annealing.

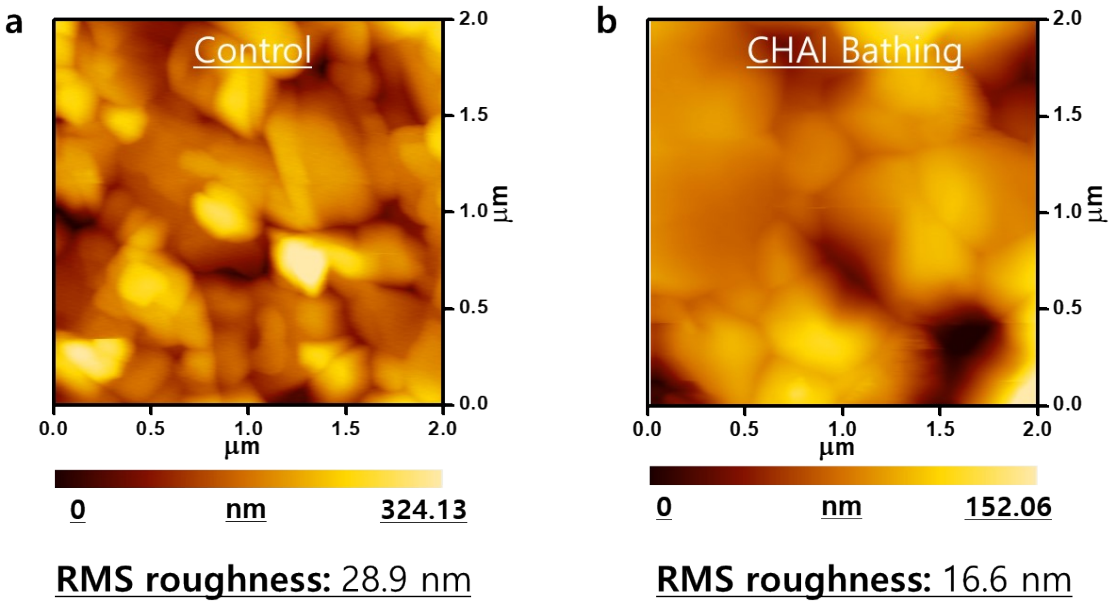


**Fig. S3** AFM images (2 µm × 2 µm) of perovskite films fabricated through (a) conventional antisolvent bathing and (b) antisolvent bathing involving an additive.

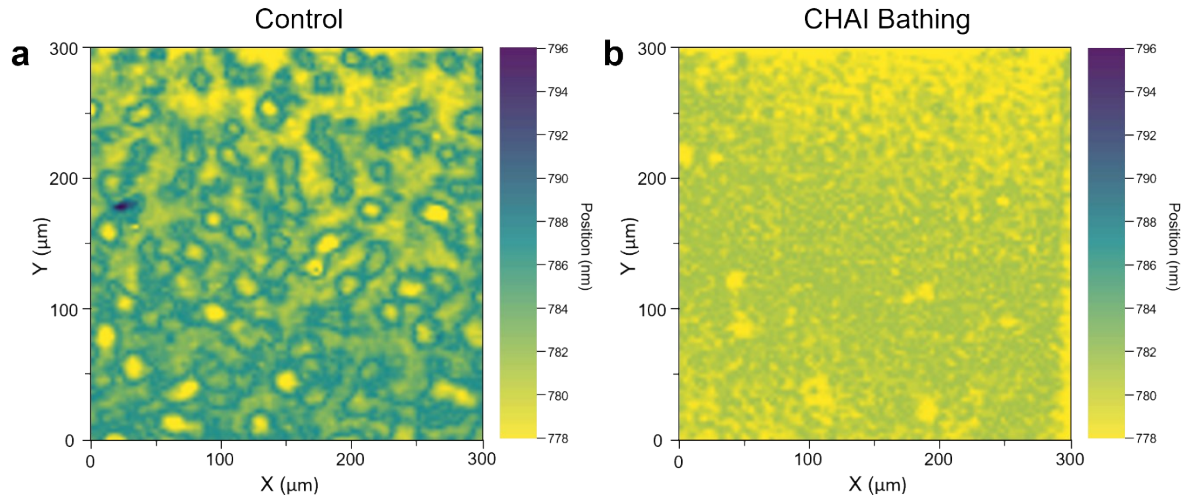


**Fig. S4** PL mapping images of the (a) control and (b) CHAI-bathed films.

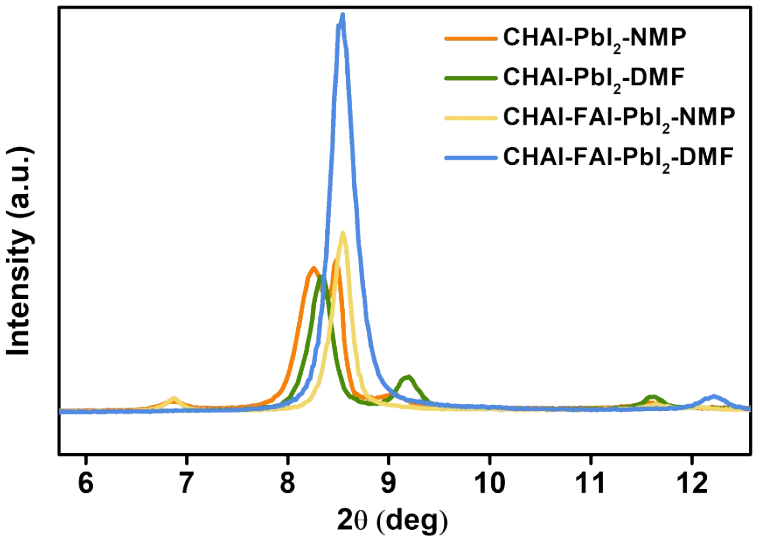


**Fig. S5** XRD spectra of CHAI–$PbI_2$–NMP, CHAI–$PbI_2$–DMF, CHAI–FAI–$PbI_2$–NMP, and CHAI–FAI–$PbI_2$–DMF intermediate phases.

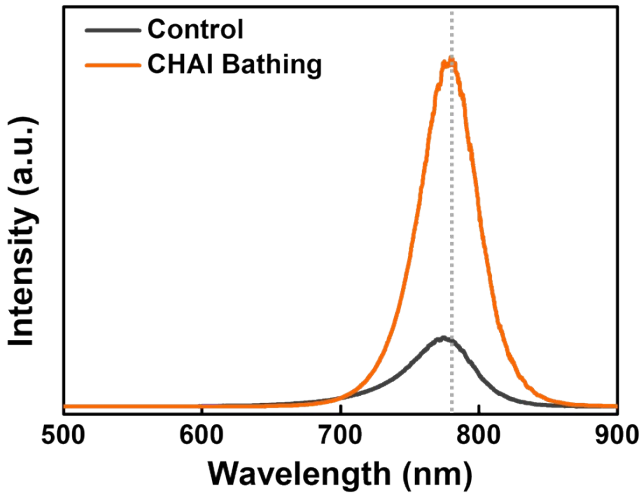


**Fig. S6** Steady-state PL spectra of the control and CHAI-antisolvent-bathed perovskite films before annealing.

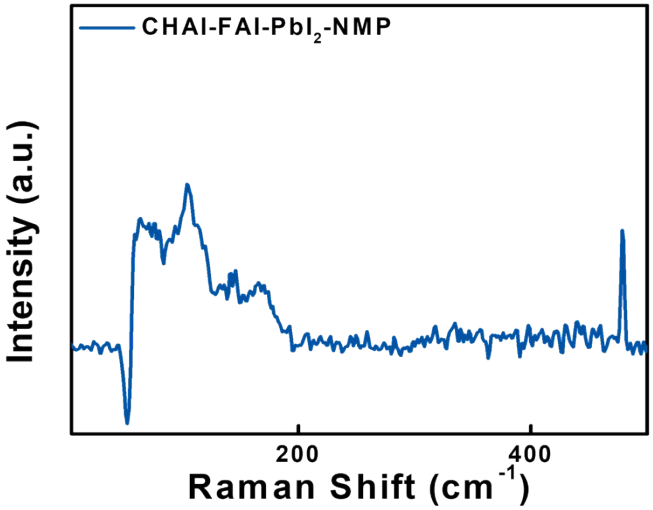


**Fig. S7** Raman spectrum of the CHAI−FAI−$PbI_2$−NMP intermediate phase.

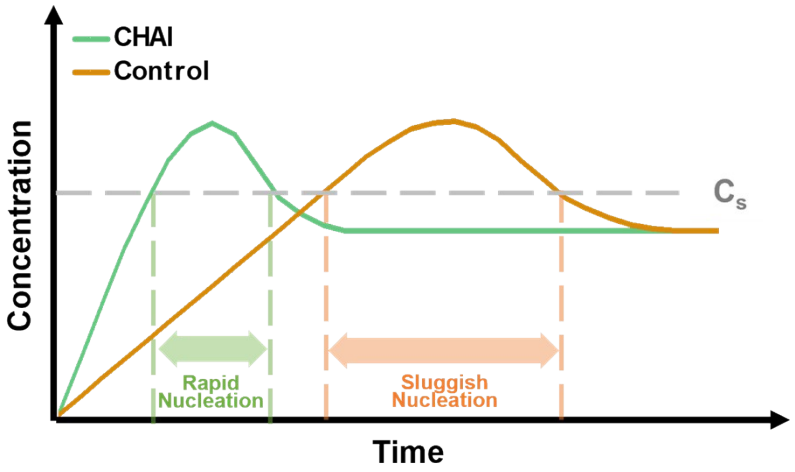


**Fig. S8** Schematics of the nucleation kinetics for the control and CHAI-bathed LHP films on the basis of the LaMer model.

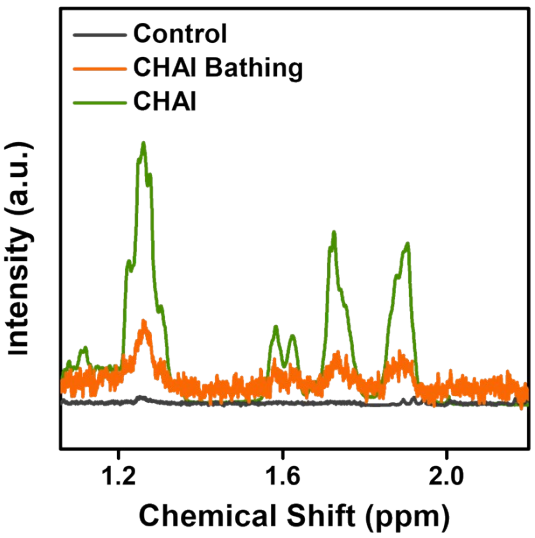


**Fig. S9** $^{1}$H-NMR spectra of the control and CHAI-bathed LHP films as well as of pristine CHAI powder dissolved in DMSO-$d_6$ solvent.

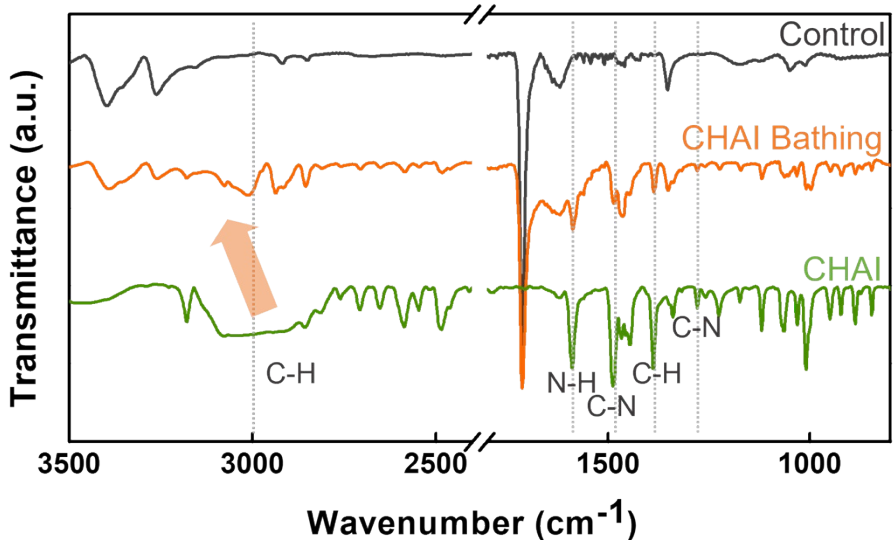


**Fig. S10** FTIR spectra of the annealed control and CHAI-bathed films and pristine CHAI powder.

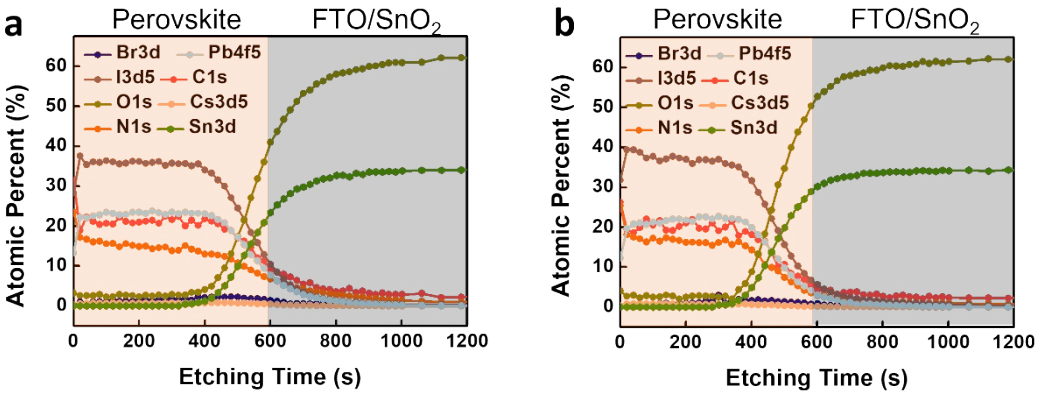


**Fig. S11** XPS depth profiles showing the atomic percentage measured for the (a) control and (b) CHAI-bathed LHP films fabricated on FTO/$SnO_2$ substrates.

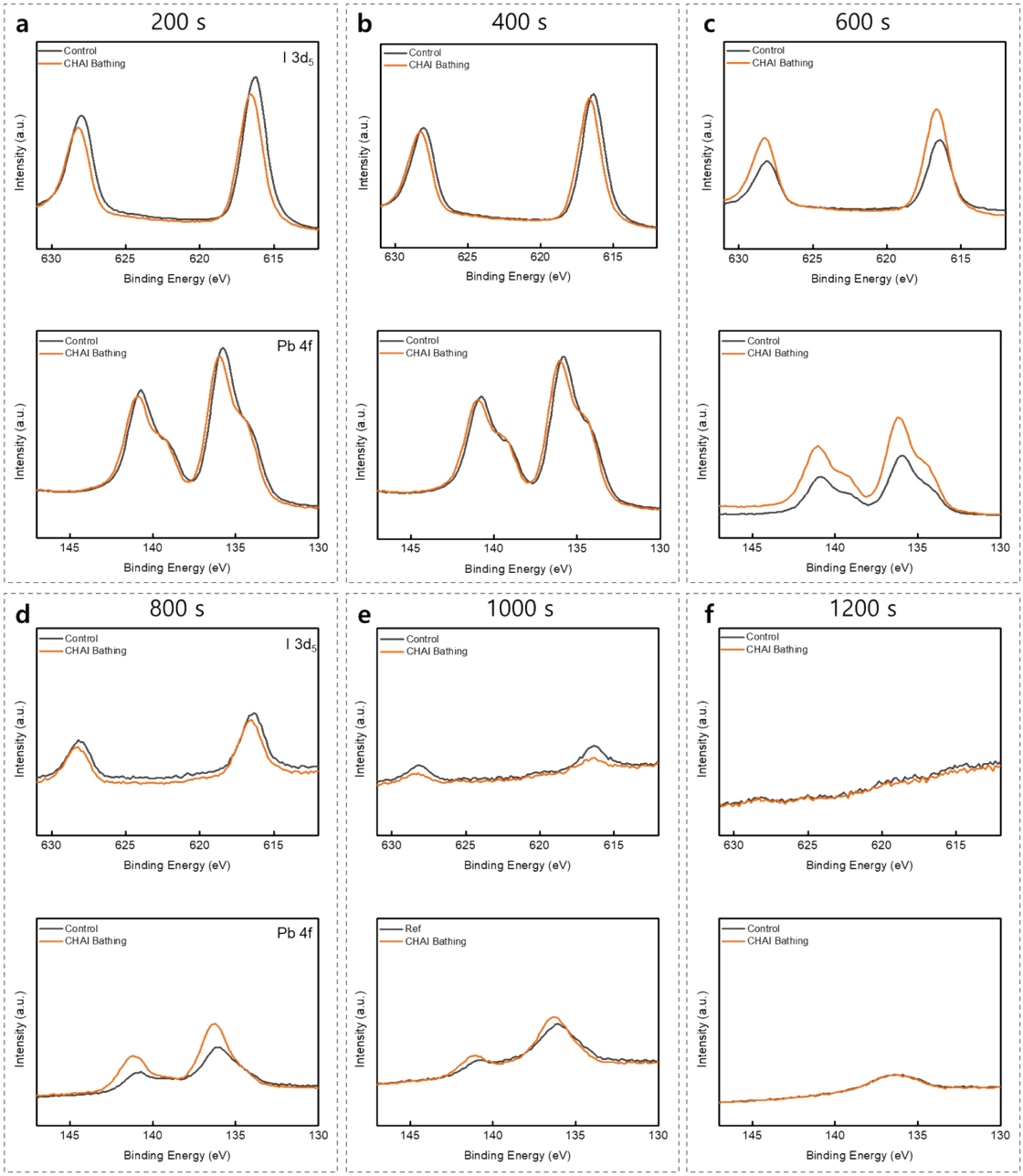


**Fig. S12** XPS depth spectra of the control and CHAI-bathed samples for different etching durations: (a) 200 s, (b) 400 s, (c) 600 s, (d) 800 s, (e) 1000 s, and (f) 1200 s. The I 3$d_5$ and Pb 4*f* peaks are shifted to a higher binding energy for a longer etching duration.

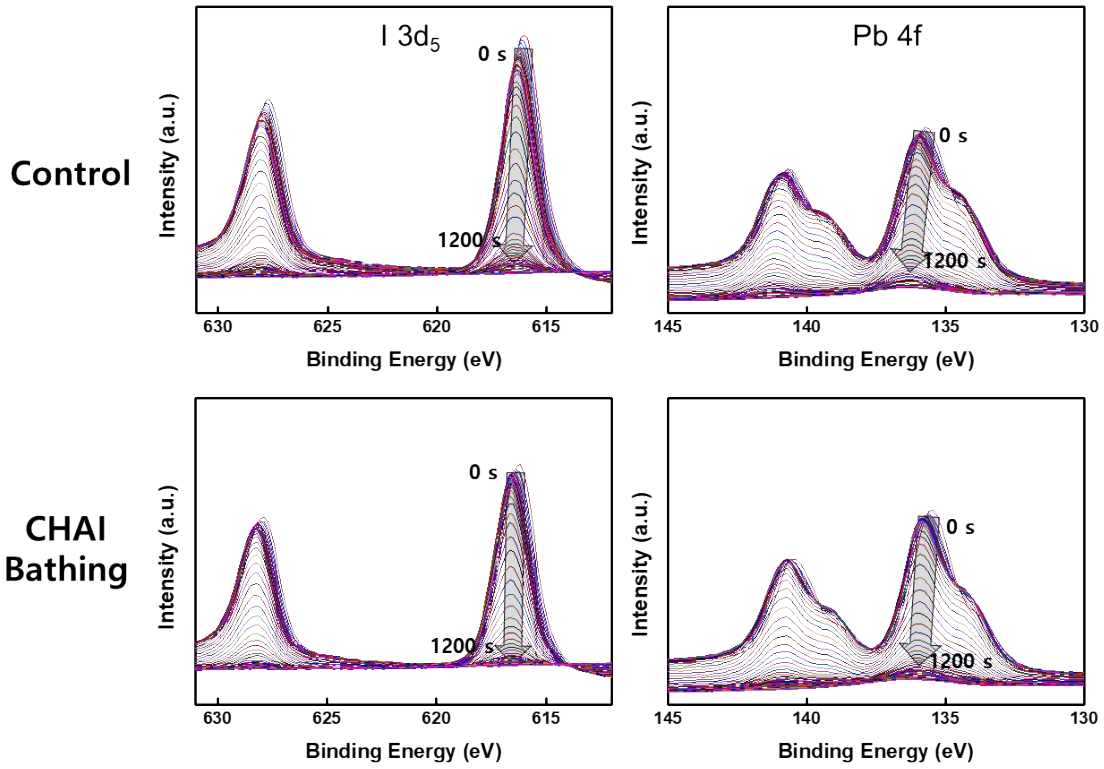


**Fig. S13** XPS depth spectra of the control and CHAI-bathed samples as a function of the etching duration (0–1200 s). Samples were etched 60 times, with a duration of 20 s for a single etching.

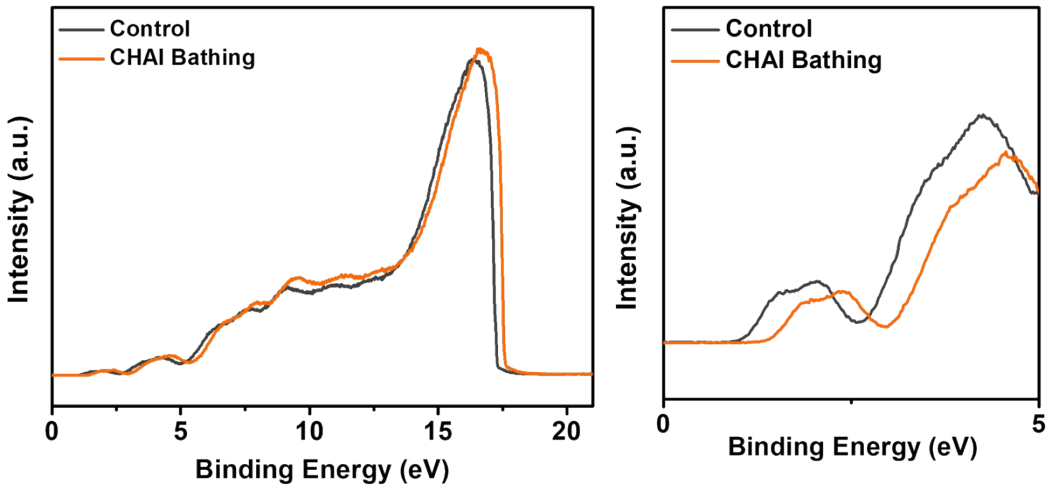


**Fig. S14** Normalized UPS spectra of the control and CHAI-bathed samples.

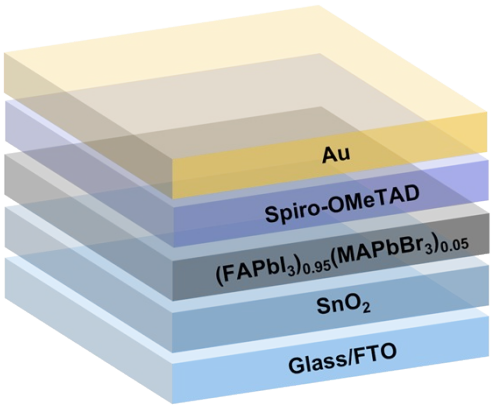


**Fig. S15** Schematic of the PSC configuration.

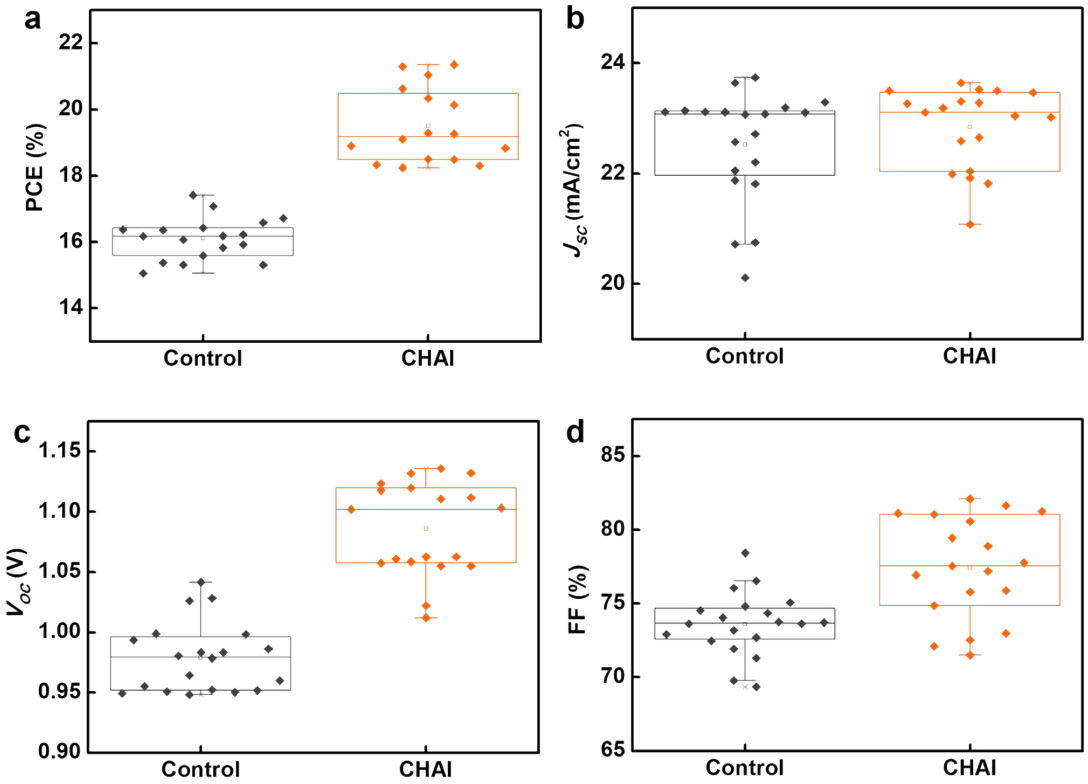


**Fig. S16** (a) PCE, (b) $J_{SC}$, (c) $V_{OC}$, and (d) FF of the 16 PSCs based on the 2 cm × 2 cm sized control and CHAI-bathed LHP films (active area of 0.06 cm$^2$). The middle dots represent the mean values, box edges represent the standard deviations, and whiskers show the maximum and minimum values in the distributions. Data are shown adjacent to the boxes.

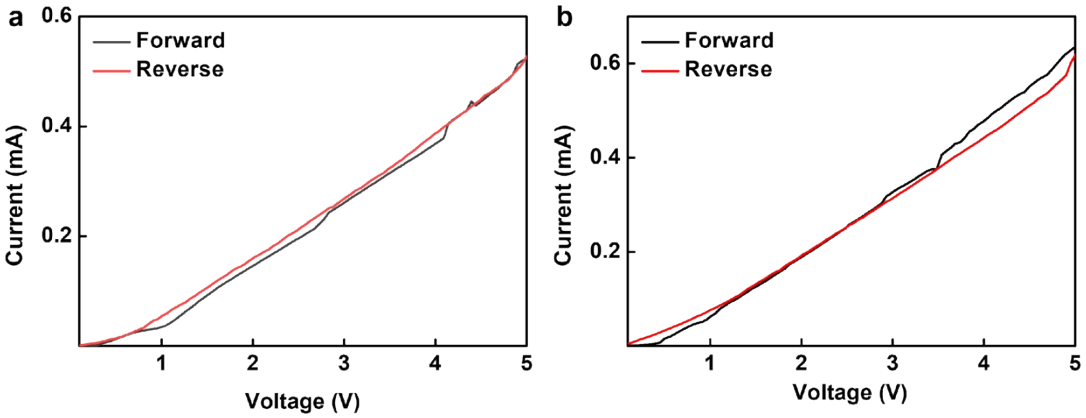


**Fig. S17** *I*–*V* curves of the (a) control and (b) CHAI-bathed LHP films for different sweeping direction (*i.e.*, forward and reverse) under dark conditions with aperture area of 0.1 $cm^2$, obtained to validate the results of SCLC analysis.

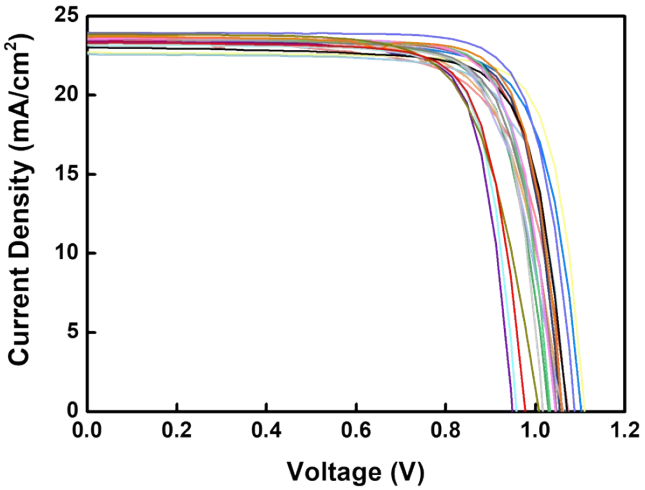


**Fig. S18** *J*–*V* curves of the 20 sub-cells (2 cm × 2 cm) of the large-area (8 cm × 10 cm) device.

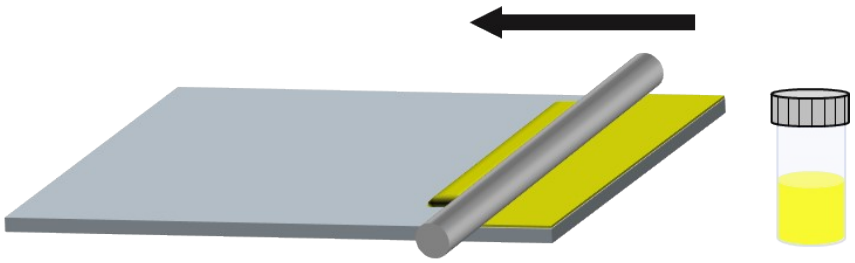

**Fig. S19** Schematic of perovskite film fabrication using bar coating method.

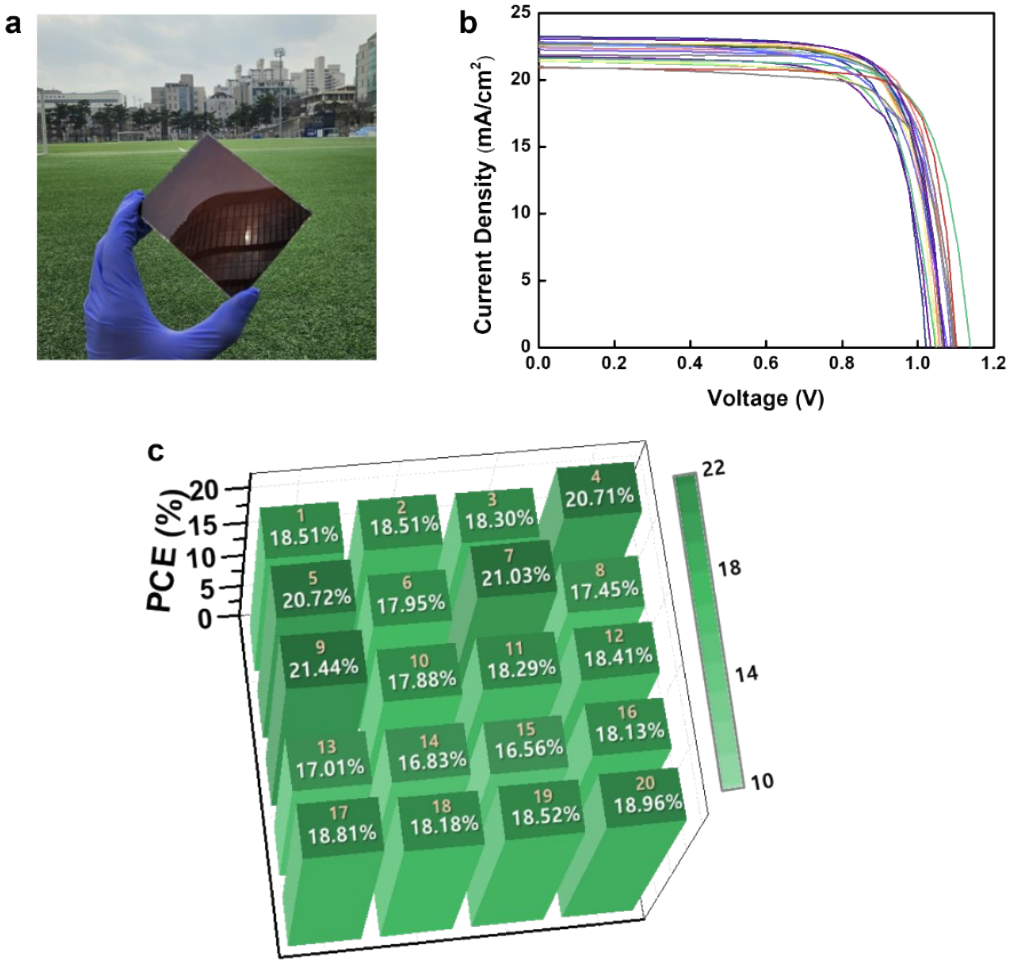


**Fig. S20** (a) A photograph of the large-area LHP films (8 cm × 10 cm) prepared with the bar coating and CHAI-bathing method. (b) A three-dimensional plot of the PCE values of PSCs depending upon the position of 20 sub-cells with 2 cm × 2 cm size. (c) *J*–*V* curves of the 20 sub-cells of the large-area (8 cm × 10 cm) device.

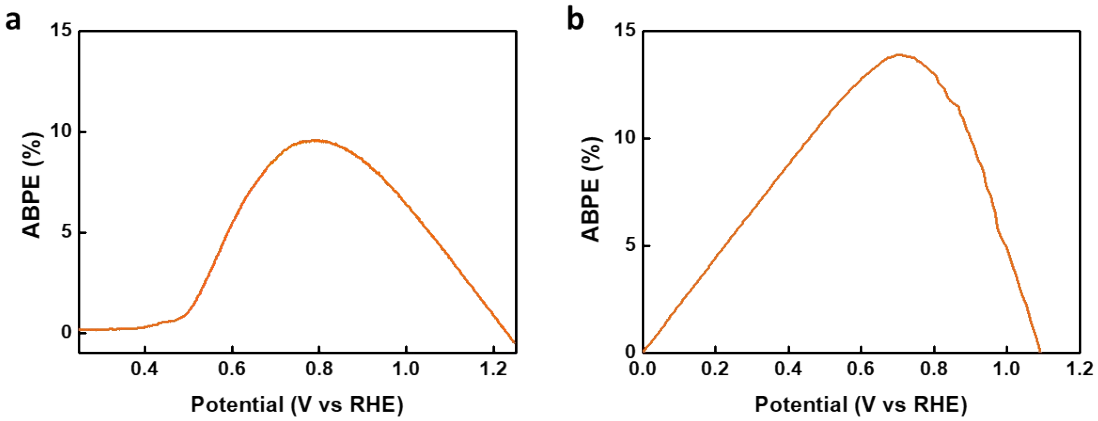


**Fig. S21** ABPE of the perovskite-based (a) photoanode and (b) photocathode measured in 1 M KOH (pH 14) and 0.5 M $H_2SO_4$ (pH 1), respectively.

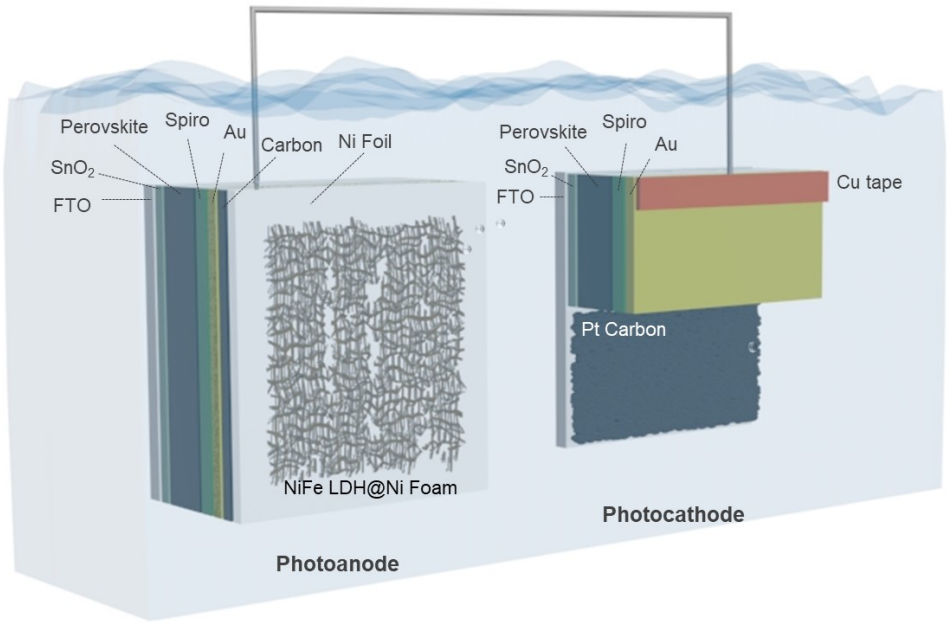


**Fig. S22** Schematic of the parallelly illuminated coplanar LHP-based photoelectrodes.

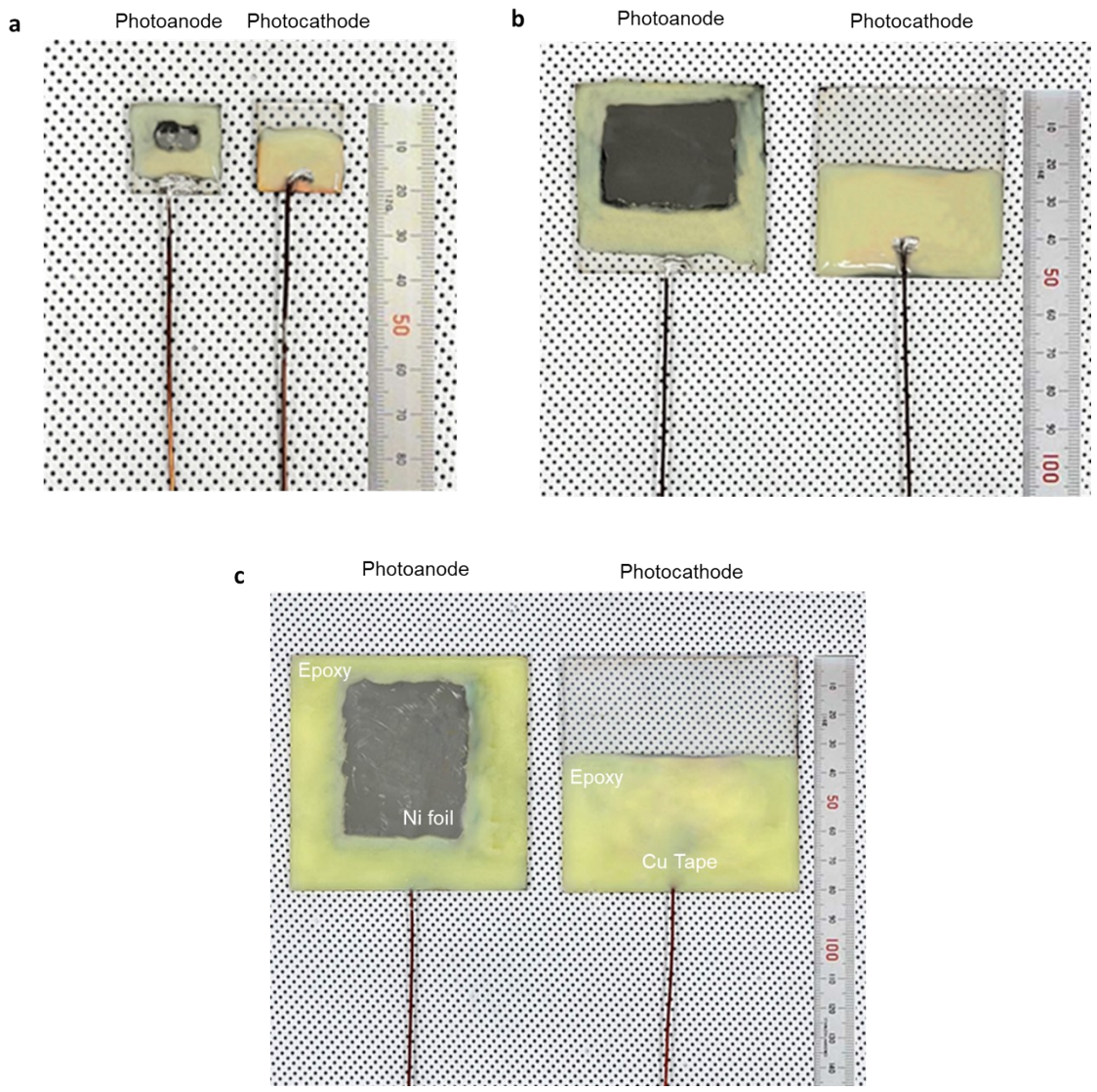


**Fig. S23** Digital photographs of the perovskite-based photoanode (FTO/$SnO_2$/LHP/spiro/carbon/Ni foil) and photocathode (FTO/$SnO_2$/LHP/spiro/Cu tape/epoxy) with different device size of (a) 2 cm × 2 cm, (b) 5 cm × 5 cm, and (c) 8 cm × 8 cm. Active area size is 0.8 $cm^2$, 12 $cm^2$, and 30 $cm^2$, respectively.

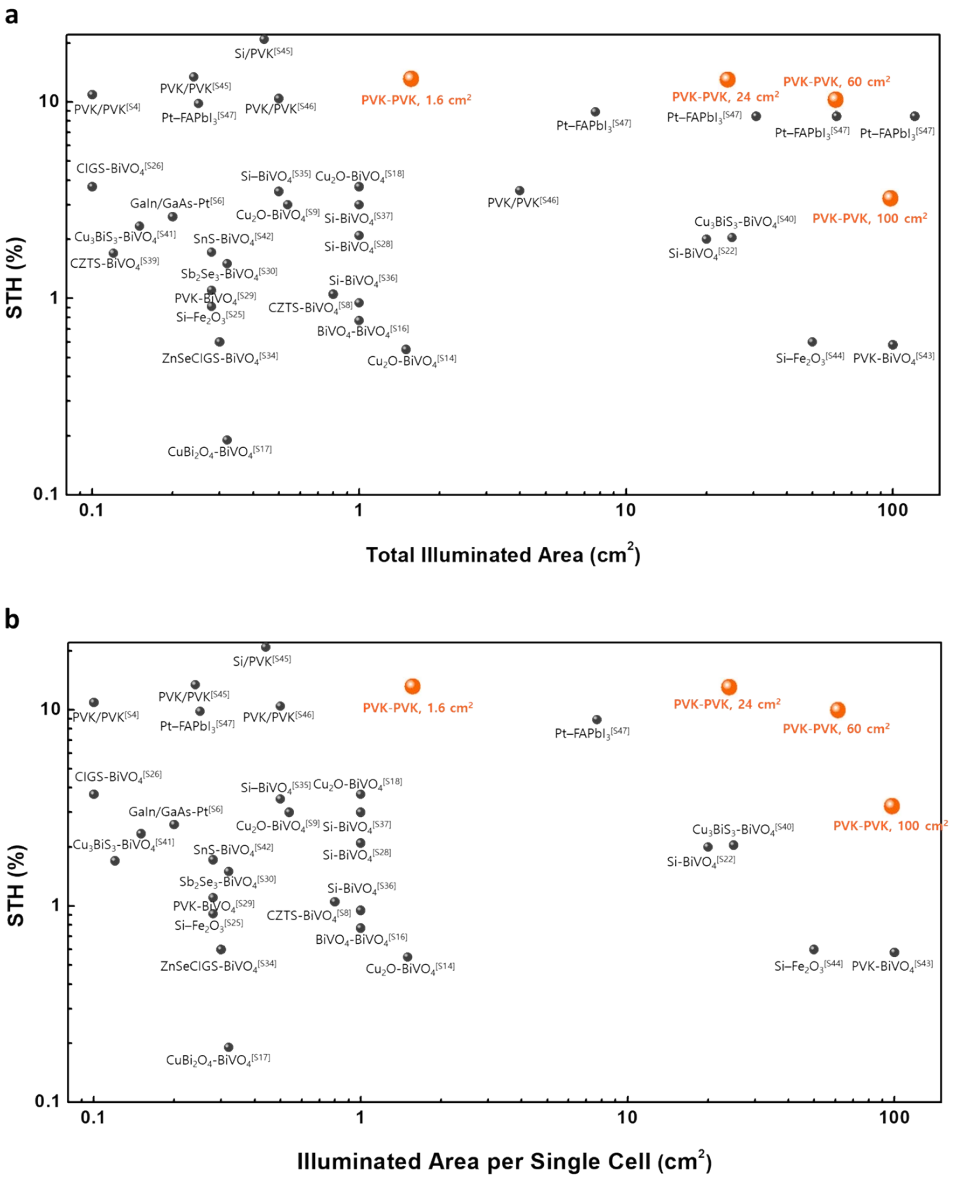


**Fig. S24** (a) STH efficiency of unbiased PEC tandems as a function of total illuminated area size. (b) STH efficiency of unbiased PEC tandems as a function of illuminated area per single cell.[S1-S47]

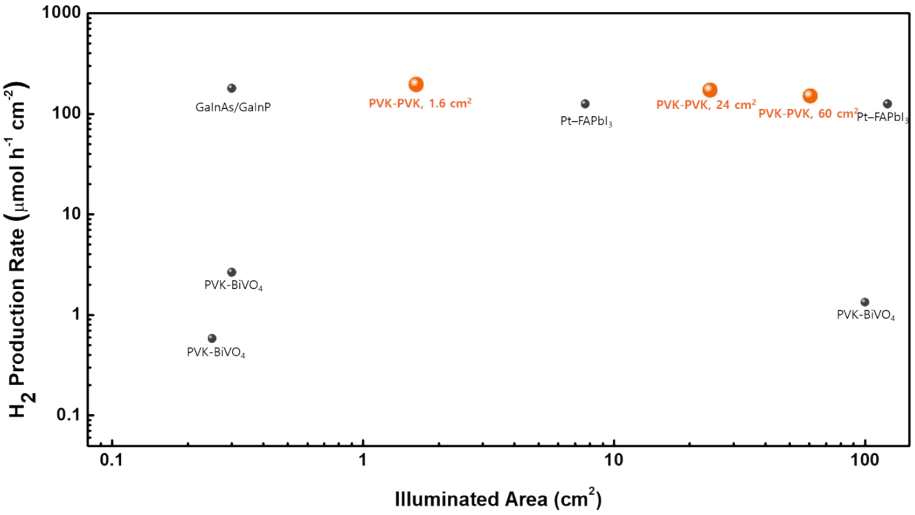


**Fig. S25** $H_2$ production rate and illumination area size benchmarks for unbiased solar water splitting under 1-sun illumination conditions.[S29, S43, S47, S48]

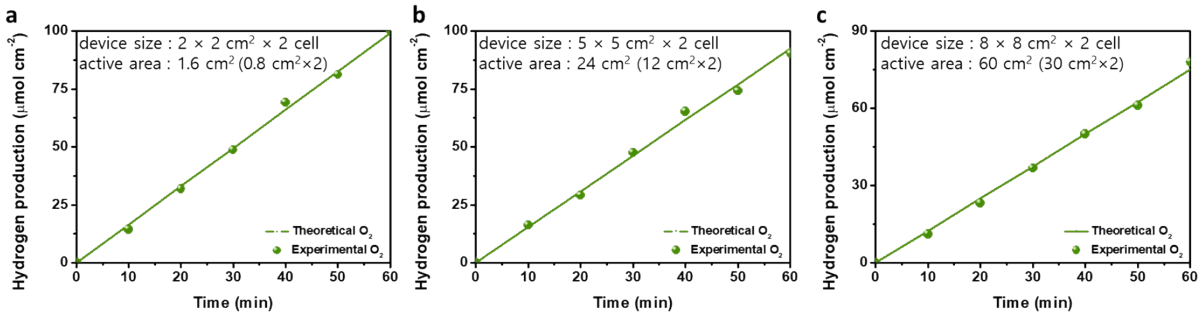


**Fig. S26** $O_2$ gas evolution rates as a function of operation time of the coplanar LHP-based photoelectrode with active area size of 1.6 $cm^2$, 24 $cm^2$, and 60 $cm^2$ under unbiased condition. The solid line indicates the calculated $O_2$ evolution rate, and the circles represent the experimental (gas chromatography) values obtained at 10 min intervals.

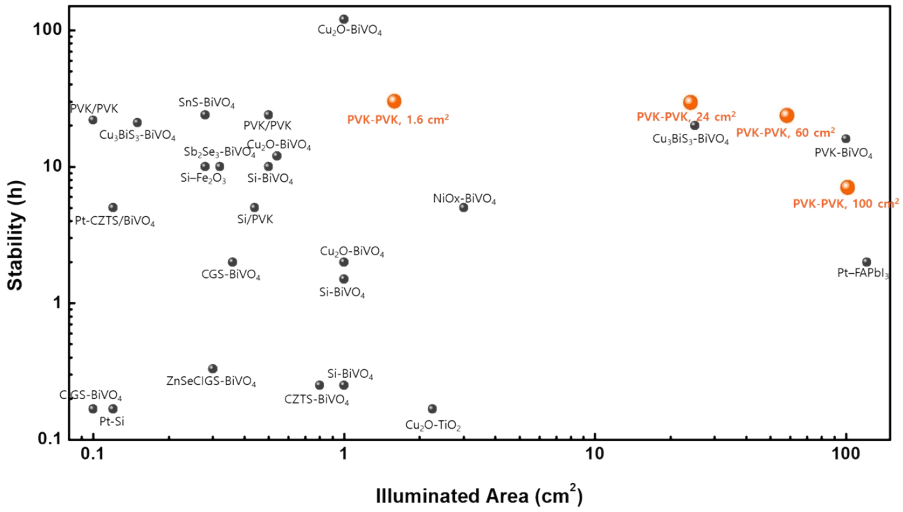


**Fig. S27** Comparison of the operation stability ($T_{80,}$ the time at which the photocurrent density drops to 80% of its initial value) and illuminated area of previously reported unbiased solar water splitting devices under 1-sun illumination conditions.[S1-S48]

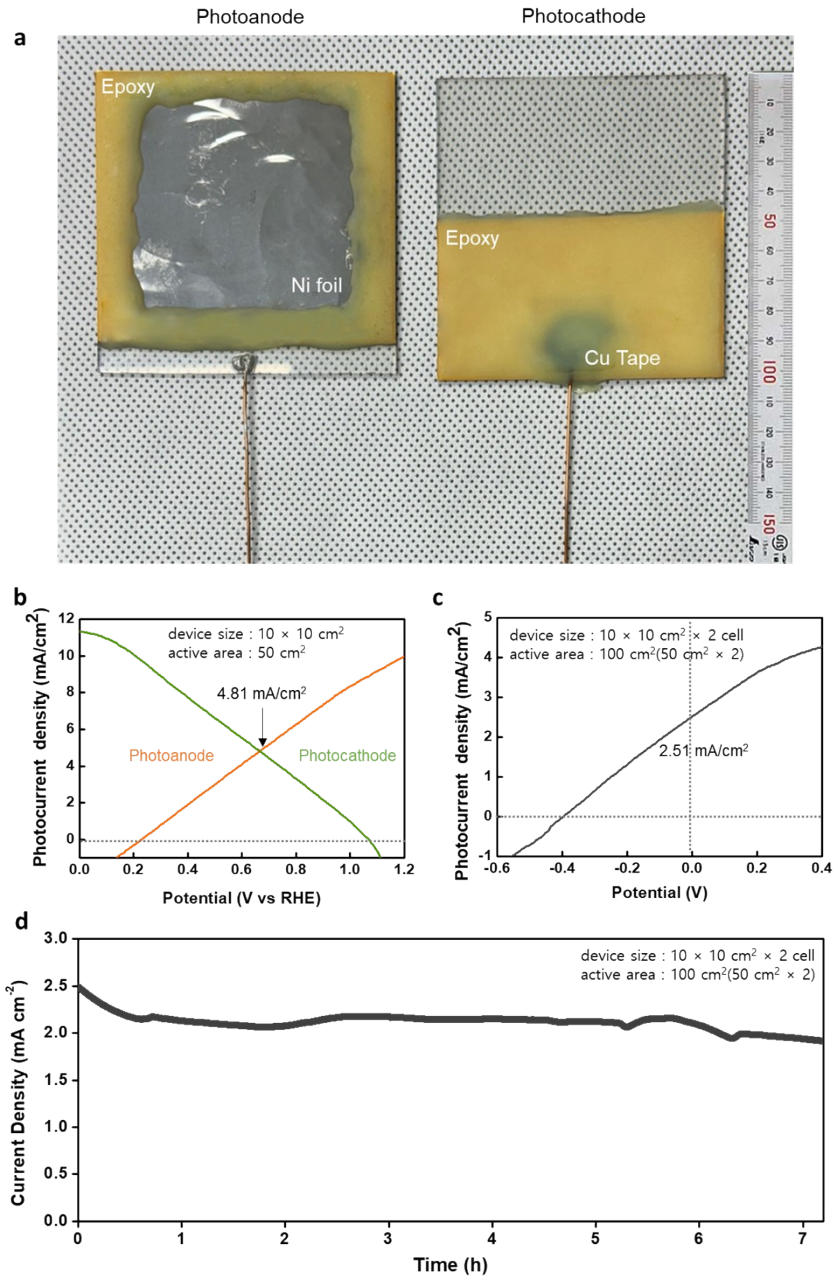


**Fig. S28** (a) Digital photographs of the large-area (10×10 $cm^2$) perovskite-based photoanode (FTO/$SnO_2$/LHP/spiro/carbon/Ni foil) and photocathode (FTO/$SnO_2$/LHP/spiro/Cu tape/epoxy). (b) LSV curves of the perovskite/Ni foil/NiFe-LDH@Ni foam photoanode and perovskite/Pt carbon photocathode under 1-sun illumination in 0.5 M KPi (pH 7). The operational point of the parallelly illuminated coplanar LHP-based photoelectrode was determined at 4.81 mA/$cm^2$. (c) LSV curve and (d) operational stability of the parallelly illuminated coplanar LHP-based photoelectrodes (a photoanode and a photocathode) in 0.5 M KPi with 1-sun illumination under a two-electrode unbiased condition (0 V).

## Supplementary Information References


S1. J. H. Kim, D. Hansora, P. Sharma, J. W. Jang and J. S. Lee, *Chem. Soc. Rev.*, 2019, **48**, 1908-1971.

S2. D. Hansora, D. Cherian, R. Mehrotra, J. W. Jang and J. S. Lee, *Joule*, 2023, **7**, 884-919.

S3. B. Liu, S. J. Wang, G. Zhang, Z. C. Gong, B. Wu, T. Wang and J. L. Gong, *Chem. Soc. Rev.*, 2023, **52**, 4644-4671.

S4. J. Yun, H. Lee, Y. S. Park, W. Jeong, C. S. Jeong, J. Lee, J. Lee, J. Tan, S. Ma, G. Jang, C. U. Lee, S. Moon, H. Im, S. Lee, D. Y. Yee, J. H. Kim and J. Moon, *Adv. Energy Mater.*, 2023, **13**. 2301693.

S5. D. W. Huang, K. Wang, L. Yu, T. H. Nguyen, S. Ikeda and F. Jiang, *ACS Energy Lett.*, 2018, **3**, 1875-1881.

S6. O. Khaselev and J. A. Turner, *Science*, 1998, **280**, 425-427.

S7. R. E. Rocheleau, E. L. Miller and A Misra, *Energy Fuels*, 1998, **12**, 3-10.

S8. J. T. Li, M. Griep, Y. S. Choi and D. Chu, *Chem. Commun.*, 2018, **54**, 3331-3334.

S9. L. F. Pan, J. H. Kim, M. T. Mayer, M. K. Son, A. Ummadisingu, J. S. Lee, A. Hagfeldt, J. S. Luo and M. Grätzel, *Nat. Catal.*, 2018, **1**, 412-420.

S10. N. Kaneza, P. S. Shinde, Y. X. Ma and S. L. Pan, *RSC Adv.* 2019, **9**, 15495-15495.

S11. C. Y. Lin, Y. H. Lai, D. Mersch and E. Reisner, *Chem. Sci.* 2012, **3**, 3482-3487.

S12. X. Yin, Q. Liu, Y. H. Yang, Y. Liu, K. K. Wang, Y. M. Li, D. W. Li, X. Q. Qiu, W. Z. Li and J. Li, *Int. J. Hydrog. Energy*, 2019, **44**, 594-604.

S13. Y. H. Huang, H. K. Yuan and H. Chen, *Molecules*, 2019, **24**. 4156.

S14. X. C. Fu, H. Chang, Z. C. Shang, P. L. Liu, J. K. Liu and H. A. Luo, *Chem. Eng. J.*, 2020, **381**, 122001.

S15. L. Tong, A. Iwase, A. Nattestad, U. Bach, M. Weidelener, G. Götz, A. Mishra, P. Bäuerle, R. Amal, G. G. Wallace and A. J. Mozer, *Energy Environ. Sci.*, 2012, **5**, 9472-9475.

S16. W. S. dos Santos, M. Rodriguez, A. S. Afonso, J. P. Mesquita, L. L. Nascimento, A. O. T. Patrocínio, A. C. Silva, L. C. A. Oliveira, J. D. Fabris and M. C. Pereira, *Sci. Rep.*, 2016, **6**, 31406.

S17. J. H. Kim, A. Adishev, J. Kim, Y. S. Kim, S. Cho, J. S. Lee, *ACS Appl. Energy Mater.*, 2018, **1**, 6694–6699.

S18. Y. Zhang, H. Lv, Z. Zhang, L. Wang, X. Wu, H. Xu, *Adv. Mater.* 2021, **33**, e2008264

S19. Y. J. Wang, Y. P. Wu, J. Schwartz, S. H. Sung, R. Hovden and Z. T. Mi, *Joule*, 2019, **3**, 2444-2456.

S20. S. Vanka, B. W. Zhou, R. A. Awni, Z. N. Song, F. A. Chowdhury, X. D. Liu, H. Hajibabaei, W. Shi, Y. X. Xiao, I. A. Navid, A. Pandey, R. Chen, C. A. Botton, T. W. Hamann, D. Wang, Y. Yan and Z. Mi, *ACS Energy Lett.* 2020, **5**, 3741-3751.

S21. J. Ziegler, B. Kaiser, W. Jaegermann, F. Urbain, J. P. Becker, V. Smirnov and F. Finger, *ChemPhysChem*, 2014, **15**, 4026-4031.

S22. A. Qayum, M. Guo, J. Wei, S. Dong, X. Jiao, D. Chen, T. Wang, *J. Mater. Chem. A*, 2020, **8**, 10989-10997.

S23. H. Döscher, J. L. Young, J. F. Geisz, J. A. Turner and T. G. Deutsch, *Energy Environ. Sci.* 2016, **9**, 74-80.

S24. M. R. Shaner, K. T. Fountaine, S. Ardo, R. H. Coridan, H. A. Atwater and N. S. Lewis, *Energy Environ. Sci.* 2014, **7**, 779-790.

S25. J. W. Jang, C. Du, Y. F. Ye, Y. J. Lin, X. H. Yao, J. Thorne, E. Liu, G. McMahon, J. F. Zhu, A. Javey, J. Guo, D. Wang, *Nat. Commun.*, 2015, **6**, 7447.

S26. H. Kobayashi, N. Sato, M. Orita, Y. Kuang, H. Kaneko, T. Minegishi, T. Yamada and K. Domen, *Energy Environ.*

*Sci.* 2018, **11**, 3003-3009.

S27. H. Li, B. Liu, S. J. Feng, H. M. Li, T. Wang and J. L. Gong, *J. Mater. Chem. A*, 2020, **8**, 224-230.

S28. B. Liu, S. J. Feng, L. F. Yang, C. C. Li, Z. B. Luo, T. Wang and J. L. Long, *Energy Environ. Sci.*, 2020, **13**, 221-228.

S29. E. E. Moore, V. Andrei, S. Zacarias, I. A. C. Pereira and E. Reisner, *ACS Energy Lett.*, 2020, **5**, 232-237.

S30. W. Yang, J. H. Kim, O. S. Hutter, L. J. Phillips, J. Tan, J. Park, H. Lee, J. D. Major, J. S. Lee and J. Moon, *Nat. Commun.*, 2020, **11**, 861.

S31. F. Jiang, Gunawan, T. Harada, Y. B. Kuang, T. Minegishi, K. Domen and S. Ikeda, *J. Am. Chem. Soc.*, 2015, **137**, 13691-13697.

S32. J. H. Kim, H. Kaneko, T. Minegishi, J. Kubota, K. Domen and J. S. Lee, *ChemSusChem*, 2016, **9**, 61-66.

S33. H. Kaneko, T. Minegishi, M. Nakabayashi, N. Shibata, Y. B. Kuang, T. Yamada and K. Domen, *Adv. Funct. Mater.*, 2016, **26**, 4570-4577.

S34. Y. Goto, T. Minegishi, Y. Kageshima, T. Higashi, H. Kaneko, Y. B. Kuang, M. Nakabayashi, N. Shibata, H. Ishihara, T. Hayashi, A. Kudo, T. Yamada, K. Domen, *J. Mater. Chem. A*, 2017, **5**, 21242-21248.

S35. S. Feng, T. Wang, B. Liu, C. Hu, L. Li, Z. J. Zhao, J. Gong, *Angew. Chem. Int. Ed.*, 2020, **59**, 2044-2048.

S36. C. M. Ding, W. Qin, N. Wang, G. J. Liu, Z. L. Wang, P. L. Yan, J. Y. Shi and C. Li, *Phys. Chem. Chem. Phys.*, 2014, **16**, 15608-15614.

S37. D. Q. Xue, M. Kan, X. F. Qian and Y. X. Zhao, *ACS Sustain. Chem. Eng.*, 2018, **6**, 16228-16234.

S38. P. Chakthranont, T. R. Hellstern, J. M. McEnaney and T. F. Jaramillo, *Adv. Energy Mater.*, 2017, **7**, 1701515.

S39. F. Jiang, C. Ozaki, Gunawan, T. Harada, Z. G. Tang, T. Minemoto, Y. Nose and S. Ikeda, *Chem. Mater.*, 2016, **28**, 3283-3291.

S40. D. Huang, L. Li, K. Wang, Y. Li, K. Feng and F. Jiang, *Nat. Commun.*, 2021, **12**, 3795.

S41. S. Moon, J. Park, H. Lee, J. W. Yang, J. Yun, Y. S. Park, J. Lee, H. Im, H. W. Jang, W. Yang and J. Moon, *Adv. Sci.*, 2023, **10**, 2206286.

S42. H. Lee, J. W. Yang, J. Tan, J. Park, S. G. Shim, Y. S. Park, J. Yun, K. Kim, H. W. Jang and J. Moon, *Adv. Sci.*, 2021, **8**, 2102458.

S43. V. Andrei, G. M. Ucoski, C. Pornrungroj, C. Uswachoke, Q. Wang, D. S. Achilleos, H. Kasap, K. P. Sokol, R. A. Jagt, H. J. Lu, T. Lawson, A. Wagner, S. D. Pike, D. S. Wright, R. L. Z. Hoye, J. L. MacManus-Driscoll, H. J. Joyce, R. H. Friend, E. Reisner, *Nature*, 2022, **608**, 518-522.

S44. A. Vilanova, T. Lopes, C. Spenke, M. Wullenkord, A. Mendes, *Energy Storage Mater.*, 2018, **13**, 175-188.

S45. A. M. K. Fehr, A. Agrawal, F. Mandani, C. L. Conrad, Q. Jiang, S. Y. Park, O. Alley, B. Li, S. Sidhik, I. Metcalf, C. Botello, J. L. Young, J. Even, J. C. Blancon, T. G. Deutsch, K. Zhu, S. Albrecht, F. M. Toma, M. Wong, A. D. Mohite *Nat. Commun.*, 2023, **14**, 3797.

S46. H. Choi, S. Seo, C. J. Yoon, J.-B. Ahn, C.-S. Kim, Y. Jung, Y. Kim, F. M. Toma, H. Kim, S. H. Lee, *Adv. Sci.,* 2023, **10**, 2303106.

S47. Cheng, W.-H., Richter, M.H., May, M.M., Ohlmann, J., Lackner, D., Dimroth, F., Hannappel, T., Atwater, H.A., and Lewerenz, H.-J. *ACS Energy Lett* .2018, 3, 1795−1800

S48. D. Hansora, J. Yoo, R. Mehrotra, W. Byun, D. Lim, Y. Kim, E. Noh, H. Lim, J. Jang, S. Seok and J. Lee, *Nat. Energy.*, 2024. [1]